Photonic crystal based polarization insensitive flat lens

2017 J. Phys. D: Appl. Phys. 50 275105

(http://iopscience.iop.org/0022-3727/50/27/275105)

IOP Publishing Journal of Physics D: Applied Physics

J. Phys. D: Appl. Phys. **50** (2017) 275105 (10pp) https://doi.org/10.1088/1361-6463/aa748b

Photonic crystal based polarization insensitive flat lens

M Turduev[1], E Bor[1,2] and H Kurt[2]

[1] Photonic Research Group, Department of Electrical and Electronics Engineering, TED University, 06420 Ankara, Turkey
[2] Nanophotonics Research Laboratory, Department of Electrical and Electronics Engineering, TOBB University of Economics and Technology, 06560 Ankara, Turkey

E-mail: mirbek.turduev@tedu.edu.tr

Received 1 February 2017, revised 8 May 2017
Accepted for publication 22 May 2017
Published 21 June 2017

Abstract

The paper proposes a new design of an inhomogeneous artificially created photonic crystal lens structure consisting of annular dielectric rods to efficiently focus both transverse electric and transverse magnetic polarizations of light into the same focal point. The locations of each individual cell that contains the annular dielectric rods are determined according to a nonlinear distribution function. The inner and outer radii of the annular photonic dielectric rods are optimized with respect to the polarization insensitive frequency response of the transmission spectrum of the lens structure. The physical background of the polarization insensitive focusing mechanism is investigated in both spatial and frequency domains. Moreover, polarization independent wavefront transformation/focusing has been explored in detail by investigating the dispersion relation of the structure. Corresponding phase index distribution of the lens is attained for polarization insensitive normalized frequency range of $a/\lambda = 0.280$ and $a/\lambda = 0.300$, where a denotes the lattice constant of the designed structure and λ denotes the wavelength of the incident light. We show the wave transformation performance and focal point movement dynamics for both polarizations of the lens structure by specially adjusting the length of the structure. The 3D finite-difference time domain numerical analysis is also performed to verify that the proposed design is able to focus the wave regardless of polarization into approximately the same focal point (difference between focal distances of both polarizations stays below 0.25λ) with an operating bandwidth of 4.30% between 1476 nm and 1541 nm at telecom wavelengths. The main superiorities of the proposed lens structure are being all dielectric and compact, and having flat front and back surfaces, rendering the proposed lens design more practical in the photonic integration process in various applications such as optical switch, attenuators and couplers, where the polarization insensitive focusing without any additional polarization control components plays an important role.

Keywords: photonic crystals, annular photonic crystals, photonic integrated circuits, optical beam focusing, polarization insensitive device, flat lens

(Some figures may appear in colour only in the online journal)

1. Introduction

Photonic crystals (PCs) are periodically designed artificial structures that consist of dielectric materials having different lattice symmetry to manipulate the propagation of photons. The spatial periodicity of PCs can be in one, two or three dimensions [1–3]. Since their proposal, PCs have attracted great interest and have been heavily studied to implement various designs and applications including reflector, waveguide, cavity, lens, sensor, laser, splitter, single photon trapping/emitting structures and schemes for obtaining slow light [4–15]. Also, PCs can exhibit unique light behaviours

such as slow light, self-collimation, superprism and negative refraction [16–22].

Even though PCs are photonic band gap based structures, they have different properties that draw the attention in addition to the presence of their band gap. The most important one of these properties is the focusing of light by a judiciously designed PC structure, which can be considered as a lens. Many focusing devices are designed by using PCs with diverse approaches. For example, graded-index (GRIN) PCs are designed to be utilized as beam bending and focusing devices [8, 23–26]. In a recent work presented in [27], a photonic optimization approach based on the differential evolution algorithm is used to design a PC structure that has the ability of subwavelength $\lambda/5$ focusing of light. Also, there are other approaches that can be followed to design a special form of focusing elements such as diffractive optical elements and kinoform lenses [28, 29].

As the propagating light interacts with material medium, the different polarizations such as transverse magnetic (TM) and transverse electric (TE), can be affected differently. A similar situation is valid for 2D PCs as well. So far, most of the studies that have been conducted on PCs deal with only one polarization of light, either TM or TE. Futhermore, polarization insensitive PC structures that similarly affect both polarizations can be designed as photonic devices. For this reason, annular photonic crystals (APCs) are introduced to control the TM and TE polarizations simultaneously [30]. By using APCs, it is possible to obtain a complete photonic band gap. There exist different APCs with unique geometrical shape in unit cell of the structure [31]. Many studies using APCs have been carried out to obtain polarization insensitive properties of photonic devices such as self-collimation [32], slow light [33], negative refraction [34], and waveguiding [35]. The negative refraction concept in APC structures is also investigated for focusing of light [36, 37].

Light focusing elements such as optical lenses can be considered as core elements in photonic applications. Focusing has great importance in applications such as nanofabrication [38] and particle manipulation [39]. In order to implement the focusing effect in photonic applications, various notable approaches based on negative refraction [40–42], Fabry–Perot resonances [43], superlenses [44], aperiodic metallic waveguide arrays [45], metamaterials [46] and photonic nano-jets [47] have been proposed. However, despite the significant progress that has been made in these studies, nearly all of the designed light focusing structures operate only for a specific polarizing mode. This drawback can be considered as a limitation to their applications in on-chip optical devices and optical interconnects. Hence, one can ask that if it is possible to design photonic lens with a broadband operation for both polarization modes at a common operating wavelength. In fact, such an issue was previously addressed in [48, 49], where two-dimensional (2D) metal-dielectric composite square-lattice PC structure is introduced to obtain polarization insensitive focusing of light. In another study, octagonal photonic quasicrystals are designed to obtain polarization insensitive focusing of light [50]. However, the use of a metal material may lead to undesired losses at the infrared/visible

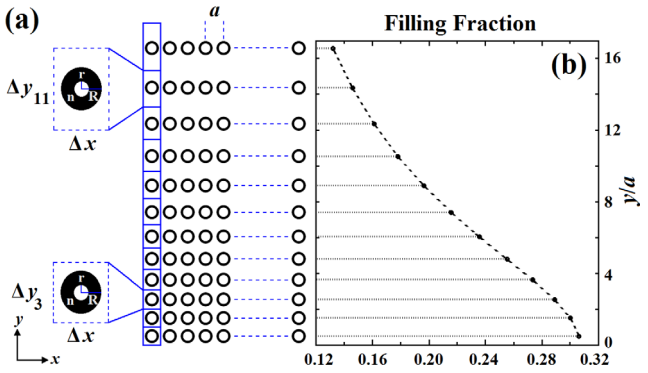

Figure 1. (a) Schematic representation of the upper half of APC (the lower half of APC structure is exact mirror symmetry of the upper half of APC with respect to x-axis) structure with parabolic lattice positions. (b) Regarding filling fraction variation along the transverse y-direction is shown. The unit cell sizes are increased along the y-direction and are kept constant to $1a$ along the x-direction. Zoomed out representation of unit cells with different lateral sizes and constant radial parameters are given as insets in (a).

wavelengths. Moreover, a photonic lens designed by octagonal quasicrystal location based approach has a large structural size, which makes it relatively impractical in terms of integrating with the photonic systems. Thus, it still remains an interesting topic whether the polarization insensitive focusing lens can be realized using all-dielectric 2D PCs which will be compact, feasible and compatible with the photonic systems.

In this paper, we introduce the design of a 2D APC lens that focuses both TM and TE polarizations into the same focal point. The effect of various inner and outer radii values of APC rods is systematically investigated. Focusing mechanisms for both polarizations are explored in detail. Lastly, the effect of the structural length on the polarization insensitive focusing behaviour is discussed. It should be noted that the preliminary data of this study was presented in an international conference [51].

2. Design approach and polarization insensitive focusing mechanisms

In this study, we have combined APC with a gradual phase index modulation concept to achieve polarization insensitive focusing using all dielectric PC structure. In this case, on one hand APCs may provide the overlapping effect of excited Bloch modes for both polarizations. On the other hand, gradual modulation manipulates phase fronts. To the best of our knowledge, this type of merging of different concepts to obtain polarization insensitive focusing has not been studied in the literature yet.

We have designed photonic medium by modulating the lattice spacing of the crystal. The designed APC lens structure consists of annular dielectric rod layers with a refractive index equal to $n = 3.13$ which corresponds to the alumina (Al_2O_3) material. We should note that the design approach is not restricted to the specified material and can be implemented using another material having a different refractive index. In each PC layer, dielectric rods are placed symmetrical to the x-axis that will be considered as the optical axis. The distance between the centers of the rods along the x-axis which belongs to the sequentially

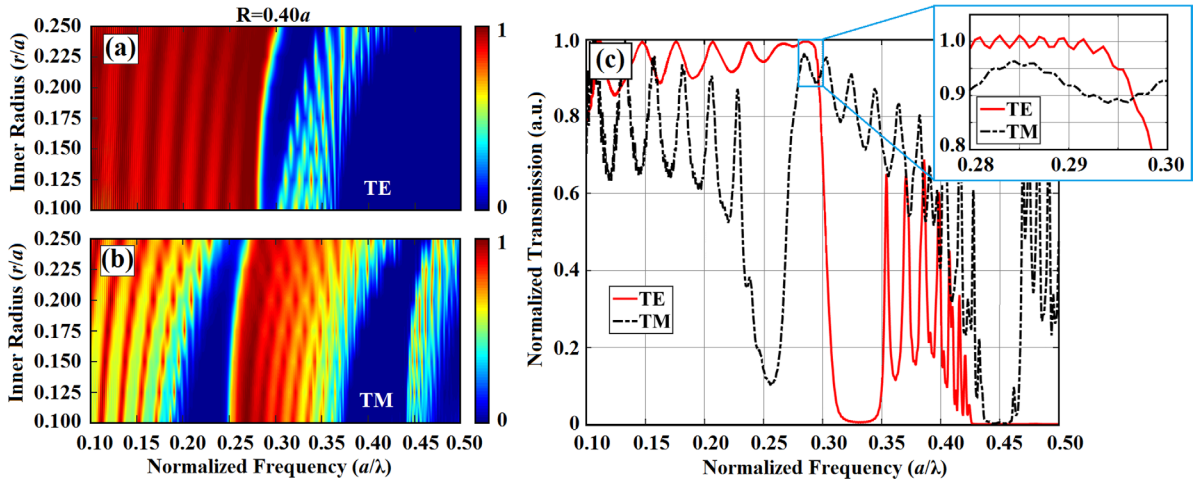

Figure 2. Normalized transmissions at different inner radii with a fixed outer radius of $R = 0.40a$ for (a) TE and (b) TM polarizations. (c) Normalized transmissions of structure with an outer radius of $R = 0.40a$ and inner radius of $r = 0.25a$ for both polarizations. The corresponding wide band high transmission interval is given as an inset.

placed columns are fixed to $1.0a$, where a denotes the lattice constant. Positions of dielectric rods along the y-direction in identical columns are determined by a parabolic function: $y_i = \alpha(y_{i-1})^2 + y_{i-1} + 2y_1$, where the positions of rods in a column in the y-direction are labelled as y_i and subscript i takes the values from 2 to 12. Hence, a single layer of APC consists of 24 annular rods in total. In this parabolic equation, α denotes a constant factor with a value of $0.001\,a^{-1}$ and y_1, which indicates the location of the first rod in the y-direction, selected as constant and independent from the formula and equals to $0.50a$. Figure 1 represents the schematic of the upper half part of the APC structure and its filling fraction plot. Corresponding variations of cell sizes in the transverse y-direction are depicted in figure 1(a) as insets. Filling fraction values are calculated using a simple relation $ff = \pi(R^2 - r^2)/(\Delta x \cdot \Delta y)$, where R, r, Δx and Δy stand for outer radius and inner radius of APC, longitudinal size and lateral size of the unit cell, respectively. According to the distribution of annular rods, the amount of dielectric material of the structure is dense at the center and become sparse along the transverse y-direction, as can be seen in figure 1(b). Therefore, the filling fraction of the unit cells decreases when the Δy lateral size of unit cells in the y-direction increase, so that a gradual modulation of the APC medium can be generated. It is important to note that the main objective of giving filling fraction is to show the gradual index modulation of the APC structure in the transverse y-direction, since we expect the phase transformation of the propagating wave in the transverse direction.

Since opto-geometric parameters of the unit cell of APC structure have critical effects in the control of high transmissivity as well as transport characteristics of light, two parameters inner (r) and outer (R) radii should be optimized. These parameters tailor the transmission spectrum to obtain an overlapping transmission region for both polarizations. Before starting with the optimization procedure, we should define the static opto-geometric parameters that come from the design constraints. Thus, to provide a desired feasibility in case of a fabrication attempt, a relation between inner r and outer R radii should be defined. A large enough R should be used, so that r can be changed through a broad range but r should not exceed some value since the generated thin veins between air background and air holes may lead to fabrication difficulties [52]. By taking these trade-offs into account, the outer radii of APC structure are fixed to $R = 0.40a$ with an inner radius r changing from $0.10a$ to $0.25a$.

To extract the transmission spectrum, finite-difference time-domain (FDTD) method with a perfectly matched layer boundary condition is used [53]. To determine TM–TE overlapping high transmission region with a fixed $R = 0.40a$ the inner radius is scanned from $r = 0.10a$ to $0.25a$ with $0.005a$ steps. The lateral and longitudinal dimensions of the considered APC structure are fixed to $L_y = 33.92a$ (24 successive PC unit cells) and $L_x = 9.8a$ (10 consecutive PC layers), respectively. Calculated transmission efficiencies are superimposed in a single transmission map as shown in figures 2(a) and (b) for TE and TM polarizations, respectively. As can be seen from figure 2(b), for TM polarizations we observe high Fabry-Perrot oscillations around the first transmission band whereas for TE polarization the oscillations are fairly low in figure 2(a). High transmission regions are observed within the normalized frequency interval of $a/\lambda = 0.10$–0.30 for TE polarization and $a/\lambda = 0.28$–0.32 for TM polarization where transmission efficiencies oscillate between 97% and 100%. Hence, the largest overlapping transmission region can be determined as the interval lying between normalized frequencies of $a/\lambda = 0.28$ and $a/\lambda = 0.30$ for the inner radius equal to $r = 0.25a$. Figure 2(c) shows the transmissions of TM and TE polarizations for the selected APC structure. The interested normalized frequency interval is given as a zoomed inset in figure 2(c). As seen in figure 2(c), the first lower band edge region of the TE mode overlaps with the second band edge of TM mode, i.e. the selected normalized frequency interval is in the first transmission band for TE polarization and in the second transmission band for TM polarization.

The proposed APC lens structure can be considered as a stack of PC unit cells in the lateral y-direction that exhibits their own dispersion properties. The difference between lateral and longitudinal dimensions of each individual PC cell provides different local group velocities for each PC unit cell. Analysis of the group velocity inside the structure can be achieved by the study of the PC's iso-frequency contours (IFCs). In this regard, to understand propagation and focusing behaviour of light, the analysis should be performed in each individual cell where information obtained from the IFCs is invaluable. These contours are the intersections of band surface and planes at a particular frequency. Moreover, calculated IFCs will give us detailed information on dispersive phenomena of the structure and may help exploring physical concept of the focusing effect of the APC structure.

To analyse the spectral response of the whole APC structure, we start with the computation of the dispersion contours corresponding for different lateral size of individual PC unit cells with $R = 0.40a$ and $r = 0.25a$. Plane wave expansion method is utilized for all IFC calculations [54]. Throughout the study, we have used freely available software called MEEP and MPB, for FDTD and PWE simulations, respectively [55, 56]. Figures 3(a)–(d) show the collection of IFCs for PC unit cells with lateral sizes equal to $\Delta y = 1.0a$ and $\Delta y = 1.30a$, where lattice sizes in the propagation direction are kept as $\Delta x = 1.0a$. We should note that the corresponding IFCs are calculated by considering the overlapping high transmission efficiency region that lies within the normalized frequency values of $a/\lambda = 0.28$ and $a/\lambda = 0.30$.

Figures 3(a) and (b) correspond to the IFC plots of the first and second band of TE and TM polarizations, respectively, where PC unit cell sizes for both polarizations are fixed to $\Delta y = 1.0a$ in the y-direction. As seen in figure 1(a), the lateral sizes of the PC unit cells increase while moving along the transverse y-axis. For this reason, to see the full picture of the spectral response of the APC structure, additional dispersion curves for the larger PC lateral size equal to $\Delta y = 1.30a$ are calculated and given in figures 3(c) and (d) for both TE and TM polarizations, respectively. IFCs for TE polarization in figures 3(a) and (c) are in circular shape which means that the APC structure can still be assumed as a homogeneous isotropic medium within the interested normalized frequency region (dashed curves). In this normalized frequency region, an APC structure can be considered as an effective medium with definite effective refractive index. Due to the gradual change in the size of the rectangular unit cells in the transversedirection, neither phase velocities nor group velocities are constant. And increase or decrease in the aspect ratio induces a variation of the effective index amount in the rectangular unit cell. Moreover, in TE polarization, while moving from the optical axis toward both upper and lower edges of the APC structure the corresponding aspect ratio gradually decreases. Hence, the effective index distribution of APC structure is higher around the center and decreases towards the edges according to the distribution of APCs. Hence, one can deduce that to produce light focusing in APC lens for TE polarization is mainly governed by the optical principles of gradual phase index modulated medium.

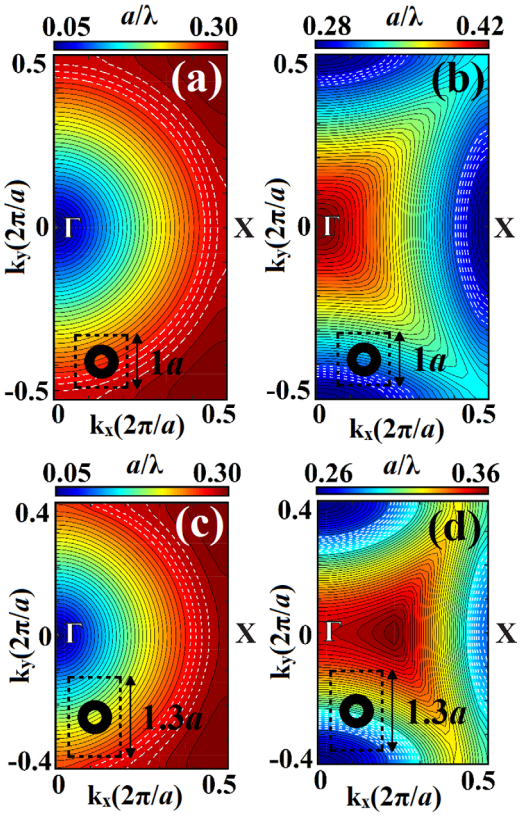

Figure 3. Representation of IFCs of unit cell with lateral size of $\Delta y = 1.0a$ for (a) first band of TE and (b) second band of TM polarizations (c) and (d) shows the first band of TE and the second band of TM polarizations when lateral sizes of APC unit cell are equal to $\Delta y = 1.30a$.

The overlapping high transmission region for TM polarization emerges after the first directional band gap as shown in figure 2(c). In the case of TM polarization,the IFCs have convex-curved shapes as seen in figures 3(b) and (d). It means that for these frequencies the Bloch modes are strongly modulated. The rectangular shape of the annular PC unit cell can modify the higher TM bands more strongly, while affecting the first TM bands very slightly (as the first bands depend basically on the symmetry of lattice and filling factor). Indeed, TM polarization curvatures of IFCs between normalized frequencies of $a/\lambda = 0.28$ and $a/\lambda = 0.30$ are no more circular as shown in figures 3(b) and (d) (dashed lines), but we see that contours for TM polarization have convex shapes.

Here, we consider the case when a TM polarized incident plane wave operating at a normalized frequency with convex shaped contour strikes an interface of an APC lens. We know that in front of the APC lens the incident light is normally diffracted since air is an isotropic homogeneous medium (circular dispersion curves). After the light enters into the APC structure, because of the convex-shaped normalized frequency curves, negative diffraction occurs and the light is forced to transform its wavefronts to the desired convex shape [57, 58]. However, the physical explanation of the polarization insensitive focusing by discussing about only IFC shapes is not sufficient because we are dealing with different dispersive phenomena for different polarizations. For this reason, below

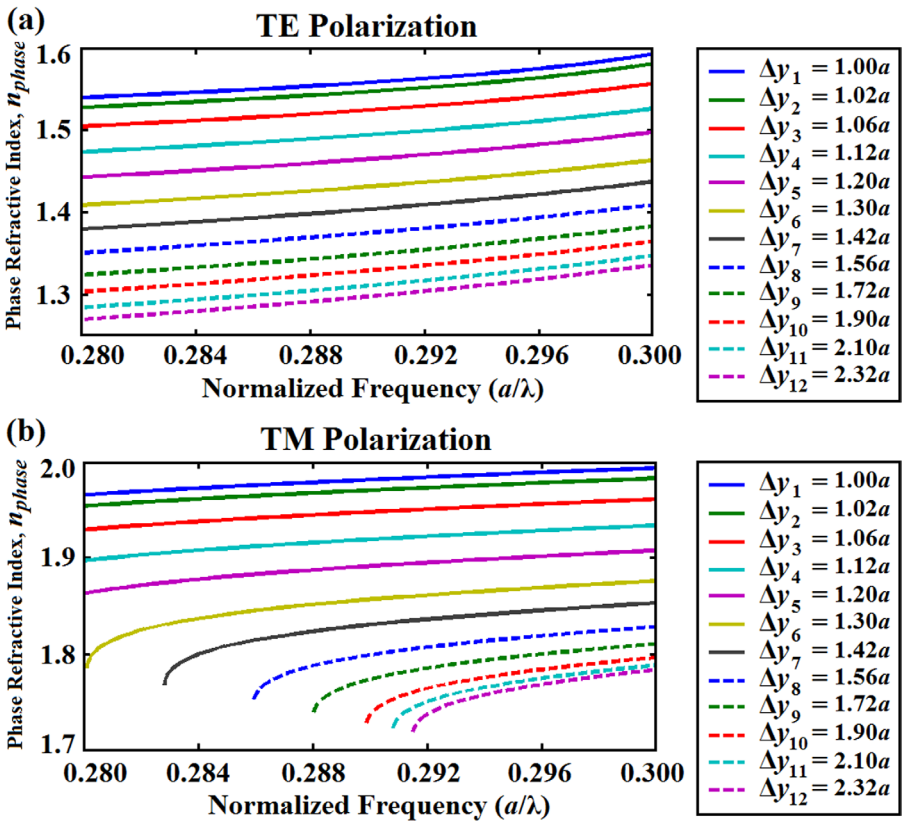

Figure 4. (a) Schematic representation of the upper-half of the APC lens structure. (b) and (c) Represents phase index variation according to frequency variations for both TE and TM polarizations, respectively.

we investigated polarization insensitive focusing characteristic of the proposed APC structure by extracting refractive index profiles for both polarizations.

The deformation of the plane wave fronts into curved/converged ones is caused by the variation of phase index of each individual unit cell of APC structure. The difference in the refractive indices induced by the lateral modulation of the unit cell sizes imposes light to travel with different optical path lengths. The differences in the optical path lengths result in wavefront deformation and wave phase retardation of the propagated beam within the PC structure. In this regard, one can deduce that the off-axis rays will experience a larger phase change than the on-axis rays due to the larger phase velocity and smaller modulus of phase index approaching near the lateral edges of the APC lens. This phase index difference makes the propagating light travel with different phase velocities. In order to show the phase index differences between the adjacent rectangular unit cells in the lateral direction within the interested polarization insensitive operating frequencies, dispersion relations of regarding unit cells are used. The dispersion diagrams yield the relations $\omega(k)$ in different directions of propagation in the crystal, where k is the propagation constant also called the wavevector. The propagation constant k corresponds to a phase velocity $\upsilon_\varphi = \omega/k$ and a phase refractive index $n_\varphi = ck/\omega$, where c is the speed of light in free space. The phase index can be determined at any point on the $\omega(k)$ dispersion curve by finding the ratio of k/ω [59].

To find the phase velocity υ_φ and the phase refractive index n_φ, the dispersion diagrams of PC unit cells with different lateral sizes are calculated by employing the plane wave expansion method in the frequency domain. Calculated dispersion diagrams of the first TE and the second TM bands are used in extraction of phase indices of each band, n_φ. The obtained phase index variation is illustrated in figures 4(a) and (b) for TE and TM polarizations, respectively. We should note that to extract the phase refractive index from the band structure of a periodic media, the band folding effect should be taken into consideration for higher bands [22]. In this context, the phase indices for the TM case are determined by unfolding the band structure at the symmetry points. As can be seen in figures 4(a) and (b), the calculated phase refractive indices covers the values between 1.25 and 1.60 for TE polarization. On the other hand, in the case of TM polarization, the phase index varies between 1.72 and 2.00. One can also relate these indices for both TE and TM polarizations with the transmission efficiency characteristic as shown in figure 2(c). Since TM polarization senses the structure as a medium with high effective refractive index at the interested frequency range comparing to TE polarization, the incident source experiences higher back-reflections in TM case so that the transmission efficiency of TM decays until 90%.

To extract the refractive index profiles of APC structure at the frequency range of $a/\lambda = 0.280$ and $a/\lambda = 0.300$, the calculated phase refractive index information in figures 4(a) and (b) are used. Fixing the operating frequency where APC

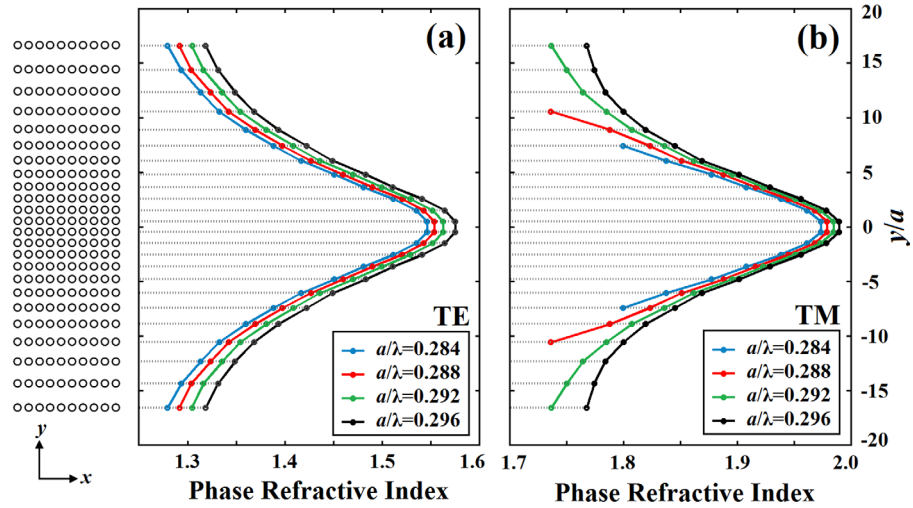

Figure 5. Representation of phase index profiles of proposed APC structure calculated within the interested frequency range of $a/\lambda = 0.284$ and $a/\lambda = 0.296$ for (a) TE and (b) TM polarizations.

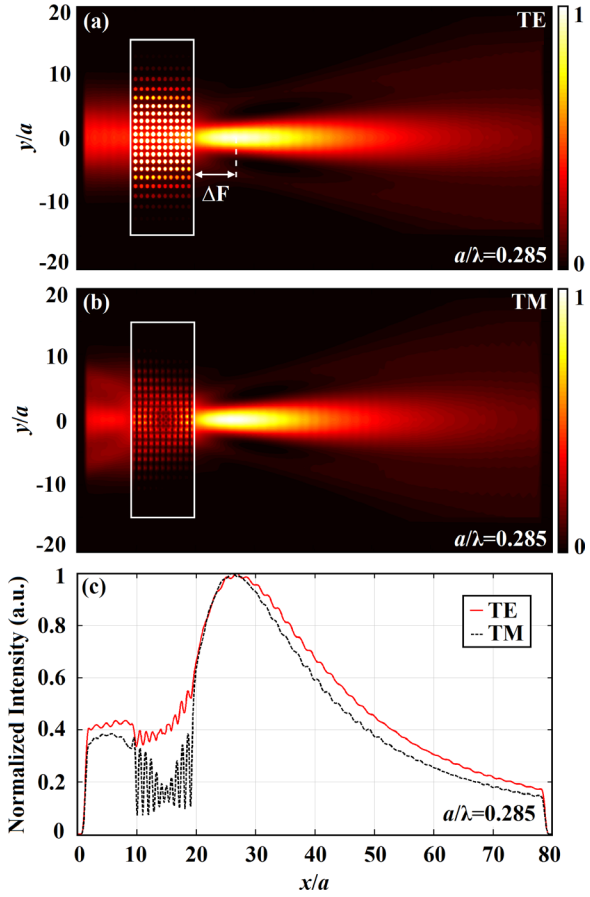

Figure 6. The spatial intensity distributions for (a) TE and (b) TM polarizations of APC structure with 10 columns (layers) that have the structural radii equal to $R = 0.40a$ and $r = 0.25a$ at the normalized frequency $a/\lambda = 0.285$. (c) On-axis intensity profiles for both polarizations.

works as polarization independent focusing lens, the phase index values of each primitive cell are collected in terms of their y-locations (dashed lines in figure 5 indicate the exact locations of PC unit cell) so that the concerning phase index profile could be generated (see figure 5). It is well known that the curvature of the phase index profile, rather than its magnitude, directly affects the light wavefront transformation of the propagating light inside the PC media. Comparing the phase index profiles for both TE and TM polarizations in figures 5(a) and (b), the trend of index variation approaching to the center of APC structure mimic each other, i.e. the gradient of the phase index profiles are similar for both TE and TM cases especially around the center of the APC structure. It can be deduced from the phase index profile calculations that the propagating light undergoes similar wavefront transformation for both polarizations that provides the overlapping of focal distances.

Next, to show the focusing mechanism in the spatial domain, the FDTD method is carried out and the proposed APC structure is tested under the excitation of TE and TM polarizations. Generated APC structure with parameters $R = 0.40a$, $r = 0.25a$, $L_y = 33.92a$ and $L_x = 9.8a$ is excited with a continuous wave source with a Gaussian profile to evaluate the focusing mechanism. To exhibit a focusing mechanism we have excited the APC structure with incident light wave operating at normalized frequency of $a/\lambda = 0.285$. Calculated spatial intensity profiles of APC structure for both TE and TM polarizations are shown in figures 6(a) and (b), respectively. In figure 6(c), on-axis intensity profiles of both polarizations are superimposed. The maximum intensity points can be identified as the focal points and the distance between the back surface of APC structure and focal point is defined as the back focal length. Throughout the study, the back focal length is denoted as ΔF (see inset of figure 6(a)). In this case, back focal lengths for TE and TM are equal to point $8.9a$ and $8.65a$, respectively. It indicates that the difference between the back focal lengths is equal to $0.25a$ so that the targeted polarization insensitive focusing is almost obtained. Detailed quantitative analysis of focal length differences for both polarizations will be given in the next section. To evaluate the focusing performance, the designed APC structures with different width sizes (different number of layers) are illuminated by a continuous light source operating at normalized frequencies varying from $a/\lambda = 0.280$ to $a/\lambda = 0.300$ with $a/\lambda = 0.001$ steps.

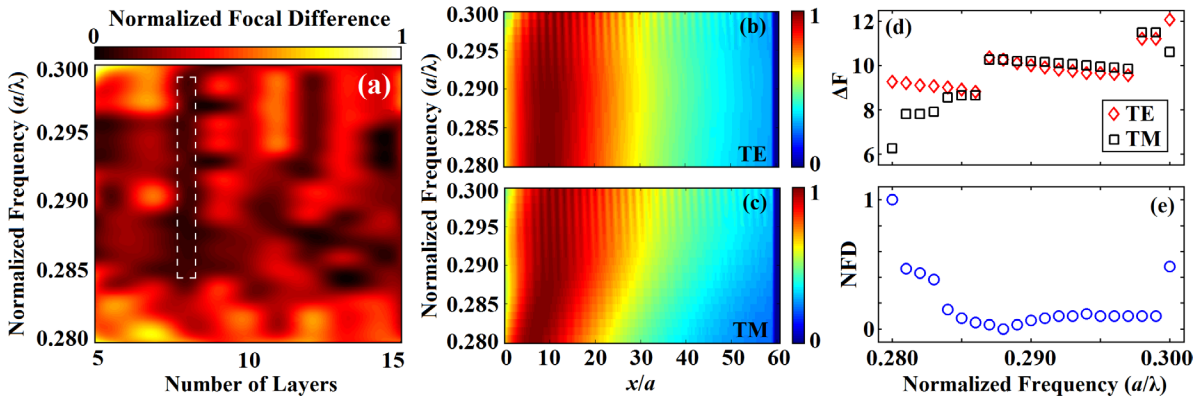

Figure 7. (a) The map of normalized NFD values for APC structures that consist of a different number of columns (layers) with radial parameters $R = 0.40a$, and $r = 0.25a$. Normalized intensity distributions after the back surface of designed structure along the optical axis, i.e. x-axis, depending on normalized frequency values for both (b) TE and (c) TM polarizations are given. Focal distances (ΔF) on normalized frequency values for both polarizations are shown in (d). Differences between focal points of both polarizations for each normalized frequency values are given in (e) as normalized values which are defined as NFD.

Table 1. Back focal length (ΔF) and FWHM deviations of the focused beam for both TE and TM polarizations operating at normalized frequency range between, $a/\lambda = 0.280$ and $a/\lambda = 0.300$ are presented.

Operating region	Freq. (a/λ)	ΔF_{TE} (a)	ΔF_{TM} (a)	$\lvert\Delta F_{TE} - \Delta F_{TM}\rvert$ (a)	$\lvert\Delta F_{TE} - \Delta F_{TM}\rvert$ (λ)	$FWHM_{TE}$ (λ)	$FWHM_{TM}$ (λ)
Lower edge	0.280	9.25	6.25	3.00	0.840	1.0780	1.0220
	0.282	9.10	7.80	1.30	0.366	1.0857	1.0434
	0.284	9.00	8.55	0.45	0.127	1.0934	1.0650
Polarization insensitive	0.285	8.90	8.65	0.25	0.071	1.0973	1.0688
focusing	0.286	8.80	8.65	0.15	0.042	1.1297	1.0688
	0.288	10.25	10.25	0.00	0.000	1.1376	1.1232
	0.290	10.00	10.20	0.20	0.058	1.1455	1.1310
	0.292	9.80	10.10	0.30	0.087	1.1242	1.1388
	0.294	9.65	10.00	0.35	0.102	1.1319	1.1319
	0.296	9.60	9.90	0.30	0.088	1.1100	1.1248
	0.298	11.20	11.50	0.30	0.089	1.1175	1.1473
	0.299	11.20	11.50	0.30	0.089	1.1212	1.1512
Upper edge	0.300	12.05	10.60	1.45	0.435	1.1250	1.1400

3. Evaluation of the numerical results

Though the designed APC structure exhibits polarization insensitive focusing, the effect of the width of structure (L_x) on the polarization insensitive focusing can be considered as an important optical parameter. For this purpose, structures that consist of a different number of layers with the rods placed along the y-axis to the same parabolic function are investigated. Dislocations of focal points for both polarizations are analysed for different structures that have a number of columns between $5a$ and $15a$. Normalized focal difference (NFD) values, which are the normalized values of the differences between back focal lengths of TE and TM polarizations, can be calculated using the following formula:

$$\mathrm{NFD} = \frac{\left|\Delta F_{\mathrm{TE}}(a/\lambda_i) - \Delta F_{\mathrm{TM}}(a/\lambda_i)\right|}{\max\left(\left|\Delta F_{\mathrm{TE}}\left(\frac{a}{\lambda_i}\right) - \Delta F_{\mathrm{TM}}\left(\frac{a}{\lambda_i}\right)\right|\right)},$$

where a/λ_i and ΔF indicates the normalized frequency values and back focal length for each polarizations, respectively. NFD values are calculated for structures with a different number of layers and given as a map in figure 7(a). The dashed dark region indicates the perfect overlapping of focal points of TE and TM polarizations. It is clear to see that there is a broad normalized frequency range, i.e. a wide dark area, for the structure with 8 layers ($L_x = 7.8a$). NFD values are normalized to the worst case in the corresponding map to compare the polarization insensitive focusing performance of structures with different number of columns. The intensity profiles along the optical axis after the back surface of the APC structure for each normalized frequency value are given as maps for TE and TM polarizations in figures 7(b) and (c), respectively. The back focal lengths for each normalized frequencies are given as a plot in figure 7(d) for both polarizations. Corresponding NFD values extracted from the figure 7(d) are given in figure 7(e). As can be seen in figures 7(d) and (e), especially between the normalized frequency values of $a/\lambda = 0.285$ and $a/\lambda = 0.299$, there occurs a perfect overlapping of focal points of both TE and TM polarizations where the focal distance differences are smaller than $0.3a$ (in terms of wavelength: 0.089λ) and corresponding NFD values are almost equal to zero. Along with the purpose of focusing TE and TM polarizations in to same focal

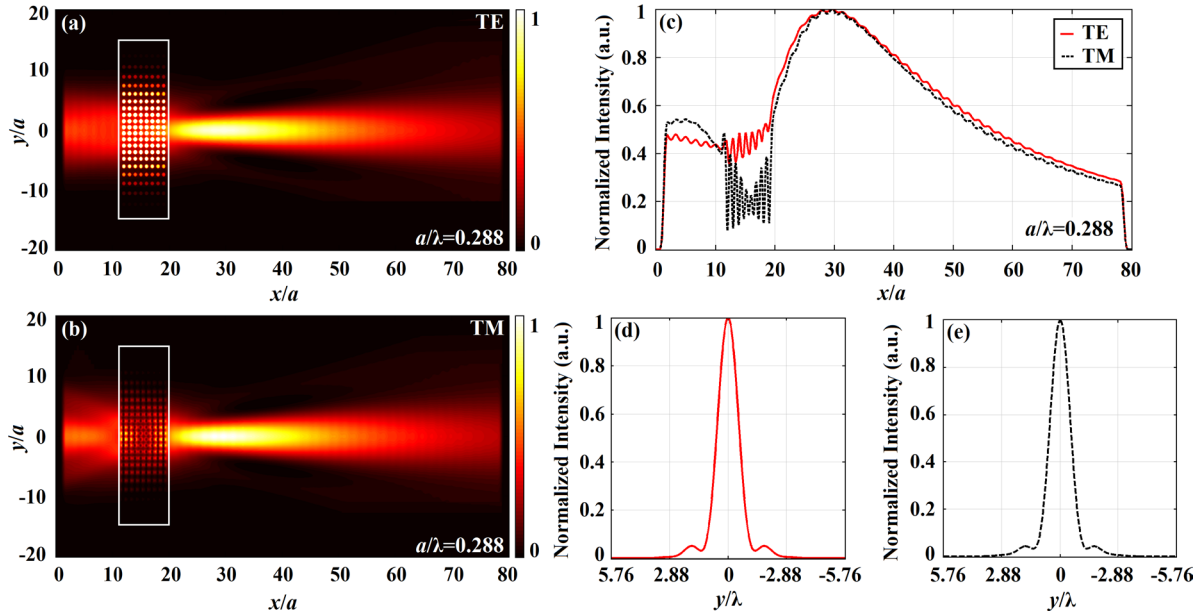

Figure 8. The spatial intensity distributions of APC structure that consist of eight columns (layers) with structural radii equal to $R = 0.40a$; $r = 0.25a$ operating at normalized frequency of $a/\lambda = 0.288$ for (a) TE and (b) TM polarizations. Corresponding on-axis intensity profiles for both TE and TM polarizations are shown in (c). The intensity profiles at the focal points are given in (d) and (e) for TE and TM, respectively.

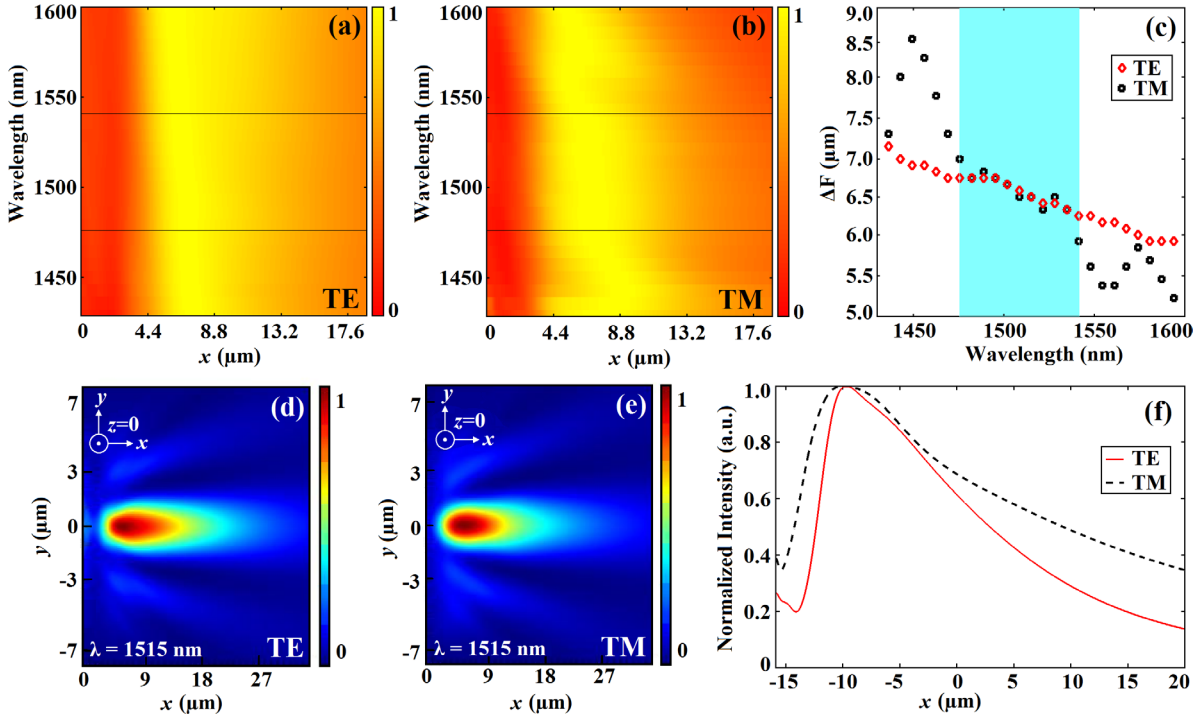

Figure 9. The on-axis cross-sections of intensity field distribution at $z = 0$ plane behind back surface of the structure are given as maps for (a) TE and (b) TM polarizations. The superimposed plots of focal distances (ΔF) versus operating wavelengths for both polarizations are shown in (c) where shaded region indicates the wavelength region of polarization insensitive focusing effect. The spatial intensity distributions ($z = 0$, $x - y$ cross-sectional plane) of the most efficient polarization insensitive focusing case are given for (d) TE and (e) TM polarizations at wavelength of 1515 nm. (f) Superimposed on-axis intensity profiles for both polarizations at wavelength of 1515 nm.

point, the similarity of the focused beam spot sizes, i.e. full width at half maximum (FWHM), can also be considered. The corresponding FWHM values at the polarization insensitive focusing frequency region are calculated. The details of these results are summarized in table 1.

As can be observed from table 1, the normalized frequency value of $a/\lambda = 0.288$ is found to be the most efficient normalized frequency value in which the polarization insensitive focusing effect with zero NFD is observed. Intensity distributions of normalized frequency value of $a/\lambda = 0.288$ for

TE and TM polarizations are given in figures 8(a) and (b), respectively. In figure 8(c), the intensity cross section at the center of the structure along the optical axis of both polarizations is given to show the overlapping focal points of both polarizations. As can be seen, the focal points of TE and TM polarizations perfectly overlap on the same focal point which is $10.25a$ away from the back surface of the APC lens structure. In figures 8(d) and (e), the transverse cross sectional profiles of focal points are given for TE and TM polarizations, respectively.

Until now, time-domain analyses are utilized for ideal 2D APC structure where the third dimension is assumed to be infinitely long. It is important to perform three-dimensional (3D) FDTD analyses to provide practical applicability of the designed polarization insensitive photonic flat lens with accurate structural dimensions in photonic integrated systems. The 3D FDTD numerical analyses are performed for both TM and TE polarization modes within the telecom wavelengths. For 3D FDTD calculations, a commercial-grade simulator called Lumerical FDTD Solutions is used [60]. Throughout the analysis, the lattice constant is fixed to $a = 445$ nm, then the structural dimensions are become as equal to 3.5 μm, 15 μm and 6.7 μm in x-, y- and z-directions, respectively. The proposed structure is illuminated by a Gaussian profile source and corresponding maps of the cross-sectional intensity profiles along the optical axis ($z = 0$, $x - y$ cross-sectional plane) are given as maps in figures 9(a) and (b), respectively. As can be seen from the plots, the extracted maps are calculated within the wavelength range of 1436 nm and 1594 nm to analyse the polarization insensitive focusing performance. Utilizing the quantitative information about focal points, the focal distances ΔF between the focal point and back focal plane versus operating wavelengths are calculated and superimposed in figure 9(c). As can be seen in figure 9(c), the shaded region defines polarization insensitive focusing region with operating bandwidth of 4.30% (65 nm) where ΔF values between two polarizations stays below 0.25λ between 1476 nm and 1541 nm. According to the plot in figure 9(c), one can observe that the proposed polarization insensitive APC structure provides the most efficient focusing effect with almost zero difference of focal distances at the operating wavelength of $\lambda = 1515$ nm. Corresponding spatial intensity distributions taken at $z = 0$, $x - y$ plane at operating wavelength of $\lambda = 1515$ nm for TE and TM polarizations are given in figures 9(d) and (e), respectively. In figure 9(f), the intensity cross section along propagation x- direction ($y = 0, z = 0$) of both polarizations is given to exhibit the overlapping focal distance for both polarizations.

4. Conclusion

In this study, the design of an APC lens structure is introduced to obtain polarization insensitive focusing of light. Focusing mechanisms for TE and TM polarizations are explained based on time and frequency domain analyses by realizing gradually variated phase index and negative diffraction effect. The overlapping of different band edges of TE and TM spectra provides an index gradient and refraction based light focusing scenario. The effect of structural parameters on obtaining polarization insensitive focusing of light is investigated. The radii values of annular rods with the inner one $r = 0.25a$ and outer one $R = 0.40a$, and number of columns equal to $8a$ are found to be the optimum values. For the designed APC structure, a bandwidth extending from $a/\lambda = 0.285$ to $a/\lambda = 0.299$ for polarization insensitive focusing is calculated as nearly 5% with respect to the center frequency of the band interval. Moreover, in order to provide realistic implementation of the proposed lens device, 3D FDTD analyses are carried out. It is calculated that the proposed design shows polarization insensitive focusing performance in telecom wavelength with operating bandwidth of 4.30% (65 nm). The designed APC lens structure has flat front and back surfaces. The properties of the designed APC structure can also pave the way for various practical applications such as optical switch, attenuators, and couplers.

Acknowledgments

MT and EB gratefully acknowledge the financial support of the Scientific and Technological Research Council of Turkey (TUBITAK), project 116F182. H K acknowledges partial support from the Turkish Academy of Sciences.

ORCID

E Bor https://orcid.org/0000-0002-1262-3761

References

[1] Joannopoulos J D, Johnson S G, Winn J N and Meade R D 2008 *Photonic Crystals: Molding the Flow of Light* (Princeton, NJ: Princeton University Press)
[2] Yablonovitch E 1987 *Phys. Rev. Lett.* **58** 2059
[3] John S 1987 *Phys. Rev. Lett.* **58** 2486
[4] Fink Y, Winn J N, Fan S, Chen C, Michel J, Joannopoulos J D and Thomas E L 1998 *Science* **282** 1679
[5] Watanabe Y, Ikeda N, Takata Y, Kitagawa Y, Ozaki N, Sugimoto Y and Asakawa K 2008 *J. Phys. D: Appl. Phys.* **41** 175109
[6] Zhou W, Qiang Z and Chen L 2007 *J. Phys. D: Appl. Phys.* **40** 2615
[7] Sanchis L, Cryan M J, Pozo J, Craddock I J and Rarity J G 2007 *Phys. Rev.* B **76** 045118
[8] Oner B B, Turduev M and Kurt H 2013 *Opt. Lett.* **38** 1688
[9] Zhang X 2005 *Phys. Rev.* B **71** 165116
[10] Deng K, Ding Y, He Z, Zhao H, Shi J and Liu Z 2009 *J. Phys. D: Appl. Phys.* **42** 185505
[11] Kurt H and Citrin D S 2005 *Appl. Phys. Lett.* **87** 041108
[12] Zhen Y and Li L 2005 *J. Phys. D: Appl. Phys.* **38** 3391
[13] Yu T, Zhou H, Gong Z, Yang J, Jiang X and Wang M 2008 *J. Phys. D: Appl. Phys.* **41** 095101
[14] Shih M H, Yang Y, Liu Y, Chang Z, Hsu K and Wu M C 2009 *J. Phys. D: Appl. Phys.* **42** 105113
[15] Noda S, Chutinan A and Imada M 2000 *Nature* **407** 608
[16] Baba T and Mori D 2007 *J. Phys. D: Appl. Phys.* **40** 2659
[17] Prather D W, Shi S, Murakowski J, Schneider G J, Sharkawy A, Chen C, Miao B and Martin R 2007 *J. Phys. D: Appl. Phys.* **40** 2635

[18] Gao B, Shi Z and Boyd R W 2015 *Opt. Express* **23** 6491
[19] Momeni B, Huang J, Soltani M, Askari M, Mohammadi S, Rakhshandehroo M and Adibi A 2006 *Opt. Express* **14** 2413
[20] Cabuz A I, Centeno E and Cassagne D 2004 *Appl. Phys. Lett.* **84** 2031
[21] Matsumoto T, Fujita S and Baba T 2005 *Opt. Express* **13** 10768
[22] Notomi M 2000 *Phys. Rev.* B **62** 10696
[23] Kurt H, Colak E, Cakmak O, Caglayan H and Ozbay E 2008 *Appl. Phys. Lett.* **93** 171108
[24] Centeno E, Cassagne D and Albert J-P 2006 *Phys. Rev.* B **73** 235119
[25] Turduev M, Hayran Z and Kurt H 2016 *J. Appl. Phys.* **120** 243102
[26] Chien H T and Chen C C 2006 *Opt. Express* **14** 10759
[27] Bor E, Turduev M and Kurt H 2016 *Sci. Rep.* **6** 30871
[28] Sales T R M and Morris G M 1997 *Appl. Opt.* **36** 253
[29] Vedernikov V M *et al* 2010 *Optoelectron. Instrum. Data Proc.* **46** 365
[30] Kurt H and Citrin D S 2005 *Opt. Express* **13** 10316
[31] Giden I H and Kurt H 2012 *Appl. Opt.* **51** 1287
[32] Turduev M, Giden I H and Kurt H 2012 *J. Opt. Soc. Am.* B **29** 1589
[33] Wu H, Citrin D S, Jiang L Y and Li X Y 2013 *Appl. Phys. Lett.* **102** 141112
[34] Jiang L, Wu H, Jia W and Li X 2012 *J. Appl. Phys.* **111** 023508
[35] Cicek A and Ulug B 2009 *Opt. Express* **17** 18381
[36] Xia F, Yun M, Liu M, Liang J, Kong W and Wan Y 2012 *J. Eur. Opt. Soc. Rap. Public.* **7** 12045
[37] Xia F, Jun M, Liu M, Liang J, Kong W, Tan H and Lv W 2013 *J. Appl. Phys.* **113** 013109
[38] Gramotnev D K and Bozhevolnyi S I 2010 *Nat. Photon.* **4** 83
[39] Grier D G 2003 *Nature* **424** 810
[40] Pendry J B and Ramakrishna S A 2003 *J. Phys.: Condens. Matter* **15** 6345
[41] Matsumoto T, Eom K and Baba T 2006 *Opt. Lett.* **31** 2786
[42] Fabre N, Fasquel S, Legrand C, Mélique X, Muller M, François M, Vanbésien O and Lippens D 2006 *Opto-Electron. Rev.* **14** 225
[43] Li X, He S and Jin Y 2007 *Phys. Rev.* B **75** 045103
[44] Cubukcu E, Aydin K, Ozbay E, Foteinopoulou S and Soukoulis C 2003 *Phys. Rev. Lett.* **91** 207401
[45] Verslegers L, Catrysse P B, Yu Z and Fan S 2009 *Phys. Rev. Lett.* **103** 033902
[46] Ren G, Wang C, Zhao Z, Tao X and Luo X 2012 *J. Opt. Soc. Am.* B **29** 3103
[47] Mahariq I, Kuzuoglu M, Tarman I H and Kurt H 2014 *IEEE Photon. J.* **6** 1
[48] Zhang X 2004 *Phys. Rev.* B **70** 205102
[49] Zhang X 2004 *Phys. Rev.* B **70** 195110
[50] Ren K and Ren X B 2011 *Eur. Phys. J. Appl. Phys.* **54** 10501
[51] Tellioglu B, Bor E, Turduev M and Kurt H 2016 *Proc. of the 18th Int. Conf. on Transparent Optical Networks (Trento)* (https://doi.org/10.1109/ICTON.2016.7550310)
[52] Kurt H, Hao R, Chen Y, Feng J, Blair J, Gaillot D P, Summers C, Citrin D S and Zhou Z 2008 *Opt. Lett.* **33** 1614
[53] Taflove A 2000 *Computational Electrodynamics: The Finite-Difference Time-Domain Method* (Norwood, MA: Artech House)
[54] Ho K M, Chan C T and Soukoulis C M 1990 *Phys. Rev. Lett.* **65** 3152
[55] Oskooi A F, Roundy D, Ibanescu M, Bermel P, Joannopoulos J D and Johnson S G 2010 *Comput. Phys. Commun.* **181** 687
[56] Johnson S G and Joannopoulos J 2001 *Opt. Express* **8** 173
[57] Maigyte L, Purlys V, Trull J, Peckus M, Cojocaru C, Gailevicius D, Malinauskas M and Staliunas K 2013 *Opt. Lett.* **38** 2376
[58] Kumar N, Herrero R, Botey M and Staliunas K 2013 *J. Opt. Soc. Am.* B **30** 2684
[59] Teich M C and Saleh B E A 2007 *Fundamentals of Photonics* (New York: Wiley)
[60] Lumerical Solutions, Inc. www.lumerical.com/tcad-products/fdtd/ (Accessed: 2 May 2017)